

## Electronic supplementary information (ESI)

### **Development of Non-Closed Silver Clusters by Transition-Metal-Coordination-Cluster Substituted Polyoxometalate Templates**

Rui Ge, Ping-Wei Cai, Cai Sun, Yan-Qiong Sun, Xin-Xiong Li\*, and Shou-Tian Zheng\*

Fujian Provincial Key Laboratory of Advanced Inorganic Oxygenated Materials, College of Chemistry, Fuzhou University, Fuzhou, Fujian 350108, China

## 1. Materials and measurements

All reagents and solvents in the experiments were commercially purchased and used without further purification.  ${}^t\text{BuC}\equiv\text{CAg}^{[1]}$  and  $\text{Na}_{10}[\text{SiW}_9\text{O}_{34}] \cdot 18\text{H}_2\text{O}^{[2]}$  and  $({}^t\text{Bu}_4\text{N})_4\text{H}_6[\text{SiW}_9\text{O}_{34}]^{[3]}$  were prepared according to the literature procedures. The composition and structure of  $({}^t\text{Bu}_4\text{N})_4\text{H}_6[\text{SiW}_9\text{O}_{34}]$  are further identified by the IR spectrum (Fig. S19) and the  ${}^{29}\text{Si}$  NMR spectrum (Fig. S20). PXRD patterns were recorded in the range 5 - 50° by using a Ultima IV diffractometer with  $\text{Cu-K}\alpha$  radiation ( $\lambda = 1.5418 \text{ \AA}$ ) and a Bruker APEX Duo CCD area diffractometer using the powder function.<sup>[4-5]</sup> IR spectra were recorded on PerkinElmer Spectrum One FT-IR infrared spectrophotometer with pressed KBr pellets in the range of 4000-500  $\text{cm}^{-1}$ . UV/Vis absorption spectra were measured on a SHIMADZU UV2600 spectrophotometer with an Integrating Sphere Attachment (ISR-2600) in the solid-state, the powder samples were held in the powdered sample holder. Morphology of the samples was measured and elemental composition analyses were conducted using an SH-4000M scanning electron microscope (SEM; HIROX Ltd., Korea) equipped with an Oxford-Horiba Inca XMax50 energy dispersive X-ray spectroscopy (EDS) attachment (Oxford Instruments Analytical, High Wycombe, England). Elemental analyses for C, H, and N were carried out on a Vario MICRO elemental analysis. Temperature-dependent photoluminescence was measured in an Edinburgh spectrofluorimeter (FLS980) coupled with an Optistat DN cryostat (Oxford Instruments), and an ITC temperature controller and a pressure gauge were used to realize the variable-temperature measurement in the range of 83-283 K. Spectra were collected at different temperatures after a 20 min homiothermy. Time-resolved photoluminescence lifetime was measured on Edinburgh spectrofluorimeter (FLS980) using a time-correlated single-photon counting technique. The temperature-dependent magnetic susceptibilities were measured by a Quantum Design MPMS device. ICP analyses were conducted on an Ultima2 spectrometer.

**Crystallography:** Crystals were collected on a Bruker APEX Duo CCD area diffractometer equipped with a fine focus, and a 2.0 kW sealed tube X-ray source ( $\text{MoK}\alpha$  radiation,  $\lambda = 0.71073 \text{ \AA}$ ) operating at 150(2) K. The empirical absorption correction was based on equivalent reflections. Structures were solved by direct methods followed by successive difference Fourier methods. Computations were performed using SHELXTL-2018 and final full-matrix refinements were against  $F^2$ . The contribution of disordered solvent molecules to the overall intensity data of structures were removed using the SQUEEZE method in PLATON. The bond valence of the incorporated TM ions was confirmed by bond valence sum calculation (Table S1). The final formulas of the compounds were determined by single-crystal XRD results combined with elemental analysis and charge balancing considerations. CCDC-2154076, 2261863, 2261850, 2154079, 2261845, 2269039, and 2154081 contain the supplementary crystallographic data for **Ag38-Zn**, **Ag38-Co**, **Ag38-Ni**, **Ag37-Zn**, **Ag36-Co**, **Ag36-Ni** and **{Ag37-Zn} $_{\infty}$** , respectively.

**Crystal data for Ag38-Zn:**  $M_r = 10851.81$ , triclinic,  $P-1$ ,  $a = 21.911(3) \text{ \AA}$ ,  $b = 23.503(3) \text{ \AA}$ ,  $c = 30.979(4) \text{ \AA}$ ,  $\alpha = 104.882(4)^\circ$ ,  $\beta = 94.518(4)^\circ$ ,  $\gamma = 92.303(4)^\circ$ ,  $V = 15340(4) \text{ \AA}^3$ ,  $Z = 2$ ,  $\rho = 2.349 \text{ g cm}^{-3}$ ,  $\text{GOF} = 1.017$ ,  $\rho(\text{max./min}) = 5.426/ -1.925 \text{ e\AA}^{-3}$ . A total of 599652 reflections were collected, 52059 of which were unique ( $R_{\text{int}} = 0.0746$ ).  $R_1(wR_2) = 0.0797 (0.2019)$  for 2238 parameters and 52059 reflections ( $I > 2\sigma(I)$ ). **For Ag38-Co:**  $M_r = 11084.92$ , triclinic,  $P-1$ ,  $a = 21.95(2) \text{ \AA}$ ,  $b = 23.43(2) \text{ \AA}$ ,  $c = 30.98(3) \text{ \AA}$ ,  $\alpha = 105.088(14)^\circ$ ,  $\beta = 94.144(13)^\circ$ ,  $\gamma = 92.363(14)^\circ$ ,  $V = 15319(24) \text{ \AA}^3$ ,  $Z = 2$ ,  $\rho = 2.403 \text{ g cm}^{-3}$ ,  $\text{GOF} = 1.018$ ,  $\rho(\text{max./min}) = 3.494/ -3.192 \text{ e\AA}^{-3}$ . A total of 318704 reflections were collected, 53219 of which were unique ( $R_{\text{int}} = 0.0923$ ).  $R_1(wR_2) = 0.0997 (0.2225)$  for 2245 parameters and 53219 reflections ( $I > 2\sigma(I)$ ). **For Ag38-Ni:**  $M_r = 11466.09$ , triclinic,  $P-1$ ,  $a = 21.941(3) \text{ \AA}$ ,  $b = 23.391(4) \text{ \AA}$ ,  $c = 30.897(5) \text{ \AA}$ ,  $\alpha = 105.433(4)^\circ$ ,  $\beta = 94.447(4)^\circ$ ,  $\gamma = 91.978(4)^\circ$ ,  $V = 15214(4) \text{ \AA}^3$ ,  $Z = 2$ ,  $\rho = 2.503 \text{ g cm}^{-3}$ ,  $\text{GOF} = 1.040$ ,  $\rho(\text{max./min}) = 5.694/ -2.699 \text{ e\AA}^{-3}$ . A total of 522184 reflections were collected, 52814 of which were unique ( $R_{\text{int}} = 0.1106$ ).  $R_1(wR_2) = 0.0936 (0.2318)$  for 2270 parameters and 52814 reflections ( $I > 2\sigma(I)$ ). **For Ag37-Zn:**  $M_r = 12631.06$ , triclinic,  $P-1$ ,  $a = 21.433(2) \text{ \AA}$ ,  $b = 25.176(2) \text{ \AA}$ ,  $c = 27.986(2) \text{ \AA}$ ,  $\alpha = 76.713(3)^\circ$ ,  $\beta = 81.315(2)^\circ$ ,  $\gamma = 83.548(3)^\circ$ ,  $V = 14481(2) \text{ \AA}^3$ ,  $Z = 2$ ,  $\rho = 2.897 \text{ g cm}^{-3}$ ,  $\text{GOF} = 1.040$ ,  $\rho(\text{max./min}) = 4.080/ -4.958 \text{ e\AA}^{-3}$ . A total of 522688 reflections were collected, 50744 of which were unique ( $R_{\text{int}} = 0.0722$ ).  $R_1(wR_2) = 0.0862 (0.1773)$  for 2691 parameters and 50744 reflections ( $I > 2\sigma(I)$ ). **For {Ag37-Zn} $_{\infty}$ :**  $M_r = 22459.97$ , Monoclinic,  $P2_1/c$ ,  $a = 24.0994(19) \text{ \AA}$ ,  $b = 38.699(3) \text{ \AA}$ ,  $c = 39.795(3) \text{ \AA}$ ,  $\alpha = 90^\circ$ ,  $\beta = 124.230(4)^\circ$ ,  $\gamma = 90^\circ$ ,  $V = 30685(4) \text{ \AA}^3$ ,  $Z = 2$ ,  $\rho = 2.431 \text{ g cm}^{-3}$ ,  $\text{GOF} = 1.551$ ,  $\rho(\text{max./min}) = 7.370/ -4.808 \text{ e\AA}^{-3}$ . A total of 772357 reflections were collected, 54669 of which were unique ( $R_{\text{int}} = 0.0927$ ).  $R_1(wR_2) = 0.1154 (0.3549)$  for 2425 parameters and 54669 reflections ( $I > 2\sigma(I)$ ). **For Ag36-Co:**  $M_r = 10970.95$ , triclinic,  $P-1$ ,  $a = 20.386(15) \text{ \AA}$ ,  $b = 21.213(17) \text{ \AA}$ ,  $c = 31.864(2) \text{ \AA}$ ,  $\alpha = 96.159(2)^\circ$ ,  $\beta = 92.500(2)^\circ$ ,  $\gamma = 105.258(2)^\circ$ ,  $V = 13180.3(17) \text{ \AA}^3$ ,  $Z = 2$ ,  $\rho = 2.764 \text{ g cm}^{-3}$ ,  $\text{GOF} = 1.063$ ,  $\rho(\text{max./min}) = 5.328/ -3.505 \text{ e\AA}^{-3}$ . A total of 406681 reflections were collected, 45516 of which were unique ( $R_{\text{int}} = 0.0592$ ).  $R_1(wR_2) = 0.0671 (0.1692)$  for 2327 parameters and 45516 reflections ( $I > 2\sigma(I)$ ). **For Ag36-Ni:**  $M_r = 13032.87$ , triclinic,  $P-1$ ,  $a = 20.495(3) \text{ \AA}$ ,  $b = 23.774(3) \text{ \AA}$ ,  $c = 31.972(4) \text{ \AA}$ ,  $\alpha = 91.397(4)^\circ$ ,  $\beta = 95.125(4)^\circ$ ,  $\gamma = 110.459(4)^\circ$ ,  $V = 14512(3) \text{ \AA}^3$ ,  $Z = 2$ ,  $\rho = 2.983 \text{ g cm}^{-3}$ ,  $\text{GOF} = 1.015$ ,  $\rho(\text{max./min}) = 4.402/ -5.533 \text{ e\AA}^{-3}$ . A total of 471758 reflections were collected, 49547 of which were unique ( $R_{\text{int}} = 0.0634$ ).  $R_1(wR_2) = 0.0984 (0.2608)$  for 2296 parameters and 49547 reflections ( $I > 2\sigma(I)$ ).

**Synthesis of Ag38-Zn:** A mixture of AgNO<sub>3</sub> (0.0169 g, 0.10 mmol), <sup>1</sup>BuC≡CAg (0.0385 g, 0.2 mmol), (<sup>1</sup>Bu<sub>4</sub>N)<sub>6</sub>H<sub>4</sub>[SiW<sub>9</sub>O<sub>34</sub>] (0.0320 g, 0.01 mmol), and Zn(Ac)<sub>2</sub>·2H<sub>2</sub>O (0.0220 g, 0.1 mmol) was dissolved in 4 mL acetonitrile. After an hour of stirring, the resulting mixture was sealed in a glass vial (20 mL) and heated at 65 °C for 1 day. After the resulting mixture cooled down to room temperature and stood for 3 days, yellow block crystals were obtained. Yield : ~ 20 mg (21.97%, based on W). Elemental analyses (based on dried sample) calcd (found %) for {[Zn<sub>4</sub>(μ<sub>3</sub>-OH)<sub>3</sub>(Ac)<sub>3</sub>SiW<sub>9</sub>O<sub>34</sub>]@Ag<sub>38</sub>(<sup>1</sup>BuC≡C)<sub>21</sub>(NO<sub>3</sub>)<sub>4</sub>CH<sub>3</sub>CN}(Ac)<sub>5</sub>: C, 18.99 (19.27); H, 2.42 (2.56); N, 0.76 (0.83), Si, 0.31(0.34), Ag, 45.03(44.78), W, 18.17 (19.01), Zn, 2.87(2.76). IR (KBr, cm<sup>-1</sup>, Fig. S21): 3435 (m), 2966 (s), 2004 (m), 1567 (s), 1412 (s), 1273 (s), 1237 (s), 1201 (m), 1026 (w), 967 (s), 910 (w), 874 (m), 792 (s), 756 (m), 667 (s), 541 (m).

**Synthesis of Ag38-Co:** The synthesis conditions were similar to those described for **Ag38-Zn**, except that Zn(Ac)<sub>2</sub>·2H<sub>2</sub>O was replaced by Co(Ac)<sub>2</sub>·4H<sub>2</sub>O. Yield: ~ 32 mg (35.25%, based on W). Elemental analyses (based on dried sample) calcd (found %) for {[Co<sub>4</sub>(μ<sub>3</sub>-OH)<sub>3</sub>(Ac)<sub>3</sub>SiW<sub>9</sub>O<sub>34</sub>]@Ag<sub>38</sub>(<sup>1</sup>BuC≡C)<sub>21</sub>(NO<sub>3</sub>)<sub>4</sub>CH<sub>3</sub>CN}(Ac)<sub>5</sub>: C, 19.05 (19.43); H, 2.43 (2.11); N, 0.77 (0.82), Si, 0.31(0.28), Ag, 45.15 (44.90), W, 18.23 (17.92), Co, 2.60(2.54). IR (KBr, cm<sup>-1</sup>, Fig. S21): 3437 (m), 2963 (s), 2006 (m), 1567 (s), 1410 (s), 1272 (s), 1236 (s), 1201 (m), 1026 (w), 963 (s), 909 (w), 868 (m), 787 (s), 750 (m), 659 (s), 538 (m).

**Synthesis of Ag38-Ni:** The synthesis conditions were similar to those described for **Ag38-Zn**, except that Zn(Ac)<sub>2</sub>·2H<sub>2</sub>O was replaced by Ni(Ac)<sub>2</sub>·4H<sub>2</sub>O. Yield: ~ 21 mg (23.14 %, based on W). Elemental analyses (based on dried sample) calcd (found %) for {[Ni<sub>4</sub>(μ<sub>3</sub>-OH)<sub>3</sub>(Ac)<sub>3</sub>SiW<sub>9</sub>O<sub>34</sub>]@Ag<sub>38</sub>(<sup>1</sup>BuC≡C)<sub>21</sub>(NO<sub>3</sub>)<sub>4</sub>CH<sub>3</sub>CN}(Ac)<sub>5</sub>: C, 19.05 (19.32); H, 2.43 (2.01); N, 0.77 (0.86), Si, 0.31(0.27), Ag, 45.16 (44.86), W, 18.23 (17.88), Ni, 2.60(2.52). IR (KBr, cm<sup>-1</sup>, Fig. S21): 3465 (m), 2966 (s), 2006 (w), 1572 (s), 1414 (s), 1272 (s), 1235 (s), 1199 (m), 1026 (w), 965 (s), 910 (w), 873 (m), 793 (s), 758 (m), 665 (s), 538 (m).

**Synthesis of Ag37-Zn:** The synthesis conditions were similar to those described for **Ag38-Zn**, except that the mixture was heated for 3 days and then placed in the dark for about two weeks. Colorless slice crystals were obtained. Yield: ~ 5 mg (9.80%, based on W). Elemental analyses (based on dried sample) calcd (found %) for {[Zn<sub>5</sub>(μ<sub>3</sub>-OH)<sub>3</sub>(Ac)<sub>2</sub>(SiW<sub>9</sub>O<sub>34</sub>)(SiW<sub>11</sub>O<sub>39</sub>)]@Ag<sub>37</sub>(<sup>1</sup>BuC≡C)<sub>22</sub>(NO<sub>3</sub>)(CH<sub>3</sub>CN)<sub>2</sub>}(NO<sub>3</sub>)·(CH<sub>3</sub>CN)<sub>2</sub>: C, 14.91 (14.65); H, 1.87 (1.94); N, 0.73 (0.68), Si, 0.49 (0.55), Ag, 34.91 (34.77), W, 32.16 (31.81), Zn, 2.86 (2.99). IR (KBr, cm<sup>-1</sup>, Fig. S22): 3465 (m), 2966 (s), 2002 (w), 1569 (m), 1452 (s), 1363 (s), 1278 (w), 1236 (s), 1201 (m), 970 (w), 906 (s), 790 (s), 723 (s), 536 (m).

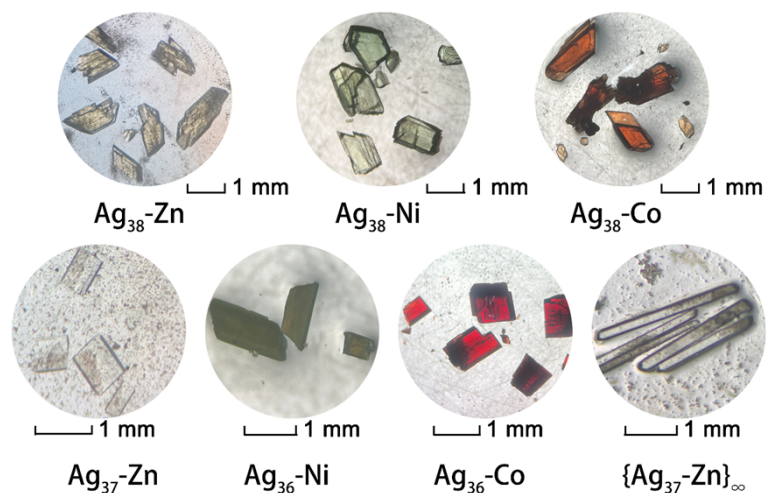
**Synthesis of Ag36-Co:** A mixture of CF<sub>3</sub>SO<sub>3</sub>Ag (0.0265 g, 0.10 mmol), <sup>1</sup>BuC≡CAg (0.0385 g, 0.2 mmol), (<sup>1</sup>Bu<sub>4</sub>N)<sub>6</sub>H<sub>4</sub>[SiW<sub>9</sub>O<sub>34</sub>] (0.0320 g, 0.01 mmol), and Co(Ac)<sub>2</sub>·4H<sub>2</sub>O (0.0130 g, 0.05 mmol) was dissolved in 4 mL acetonitrile. After an hour of stirring, the resulting mixture was sealed in a glass vial (20 mL) and heated at 65 °C for 3 days. After the resulting mixture cooled down to room temperature and stood for about one week, red block crystals were obtained. Yield: ~ 20 mg (40.10%, based on W). Elemental analyses (based on dried sample) calcd (found %) for {[Co<sub>5</sub>(μ<sub>3</sub>-OH)<sub>3</sub>(Ac)<sub>2</sub>(SiW<sub>9</sub>O<sub>34</sub>)(SiW<sub>11</sub>O<sub>39</sub>)]@Ag<sub>36</sub>(<sup>1</sup>BuC≡C)<sub>18</sub>}(Ac)<sub>5</sub>·2CH<sub>3</sub>CN: C, 13.65 (13.28); H, 1.74 (1.99); N, 0.25 (0.29), Si, 0.51(0.54), Ag, 35.03 (34.83), W, 33.17 (34.12), Co, 2.66(2.47). IR (KBr, cm<sup>-1</sup>, Fig. S22): 3477 (m), 2966 (m), 2008 (w), 1618 (w), 1560 (w), 1452 (w), 1361 (w), 1238 (m), 1200 (m), 972 (m), 891 (s), 798 (s), 706 (m), 540 (w).

**Synthesis of Ag36-Ni:** The synthesis conditions were similar to those described for **Ag36-Co**, except that Co(Ac)<sub>2</sub>·4H<sub>2</sub>O was replaced by Ni(Ac)<sub>2</sub>·4H<sub>2</sub>O. Colorless slice crystals were obtained. Yield: ~ 8 mg (16.07 %, based on W). Elemental analyses (based on dried sample) calcd (found %) for {[Ni<sub>5</sub>(μ<sub>3</sub>-OH)<sub>3</sub>(Ac)<sub>2</sub>(SiW<sub>9</sub>O<sub>34</sub>)(SiW<sub>11</sub>O<sub>39</sub>)]@Ag<sub>36</sub>(<sup>1</sup>BuC≡C)<sub>17</sub>}(Ac)<sub>6</sub>·2CH<sub>3</sub>CN : C, 13.25 (12.94); H, 1.69 (1.76); N, 0.25 (0.25), Si, 0.51(0.43), Ag, 35.10 (34.51), W, 33.24 (32.07), Ni, 2.65(2.51). IR (KBr, cm<sup>-1</sup>, Fig. S22): 3455 (w), 2965 (m), 2005 (w), 1569 (m), 1411 (s), 1361 (s), 1274 (s), 1236 (s), 1201 (m), 1022 (w), 966 (m), 914 (w), 869 (s), 790 (s), 757 (s), 663 (s), 536 (m).

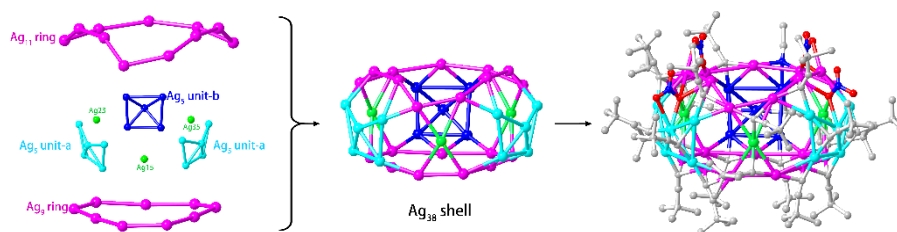
**Synthesis of {Ag37-Zn}<sub>∞</sub>:** The synthesis conditions were similar to those described for **Ag38-Zn**, except that the stoichiometric proportion of Zn(Ac)<sub>2</sub>·2H<sub>2</sub>O was reduced to half and the mixture was heated for 5 days and then placed in the dark for about two weeks. Yield: ~ 4 mg (7.92%, based on W). Elemental analyses (based on dried sample) calcd (found %) for Ag<sub>0.65</sub>{[Zn<sub>5</sub>(μ<sub>3</sub>-OH)<sub>3</sub>(Ac)<sub>2</sub>(SiW<sub>9</sub>O<sub>34</sub>)(SiW<sub>11</sub>O<sub>39</sub>)]@Ag<sub>37</sub>(<sup>1</sup>BuC≡C)<sub>19</sub>(NO<sub>3</sub>)<sub>2</sub>}(Ac)<sub>3.65</sub>: C, 13.05 (14.02); H, 1.67 (1.47); N, 0.25 (0.35), Si, 0.50 (0.63), Ag, 35.96 (36.58), W, 32.84 (32.28), Zn, 2.92 (2.67). IR (KBr, cm<sup>-1</sup>, Fig. S22): 3455 (m), 2964 (s), 2001 (m), 1575 (m), 1469 (w), 1361 (m), 1278 (m), 1236 (s), 1199 (w), 970 (m), 906 (s), 788 (s), 630 (w), 518 (s).

Fig. S23 – S29 show the ellipsoid mode of the seven compounds, and the PXRD patterns are displayed in Fig. S30 – S34. Fig. S35 – S38 exhibit the UV-vis absorption spectra of the seven clusters.

## 2. Additional figures and characterizations



**Fig. S1.** Photographs of the crystals  $\text{Ag}_{38}\text{-Zn}$ ,  $\text{Ag}_{38}\text{-Co}$ ,  $\text{Ag}_{38}\text{-Ni}$ ,  $\text{Ag}_{37}\text{-Zn}$ ,  $\text{Ag}_{36}\text{-Co}$ ,  $\text{Ag}_{36}\text{-Ni}$  and  $\{\text{Ag}_{37}\text{-Zn}\}_\infty$ .



**Fig. S2.** The structure of  $\{\text{Ag}_{38}\}$  shell. Different  $\text{Ag}^+$  ions are drawn in specific colors for clarity.

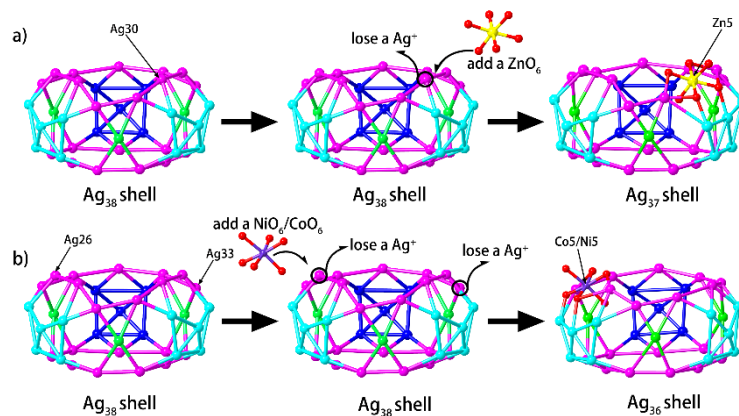


**Fig. S3.** The evolution of  $\{\text{Ag}_{37}\}$  a) and  $\{\text{Ag}_{36}\}$  b) shells from the  $\{\text{Ag}_{38}\}$  shell. All external organic ligands are omitted and different  $\text{Ag}^+$  ions are drawn in specific colors for clarity.

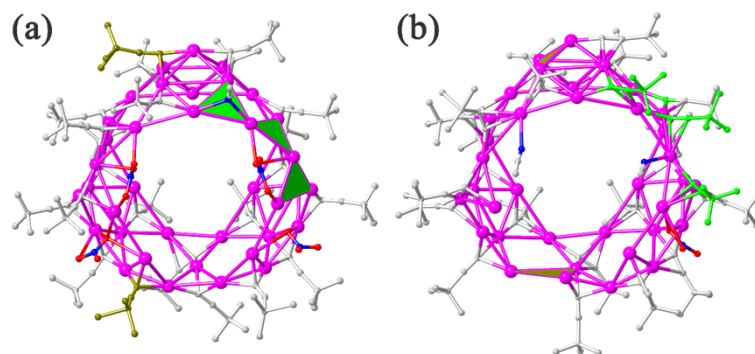


**Fig. S4.** The differences of peripheral ligands in  $\text{Ag}_{38}\text{-Zn}$  (a) and  $\text{Ag}_{37}\text{-Zn}$  (b), which are marked in green and olive.

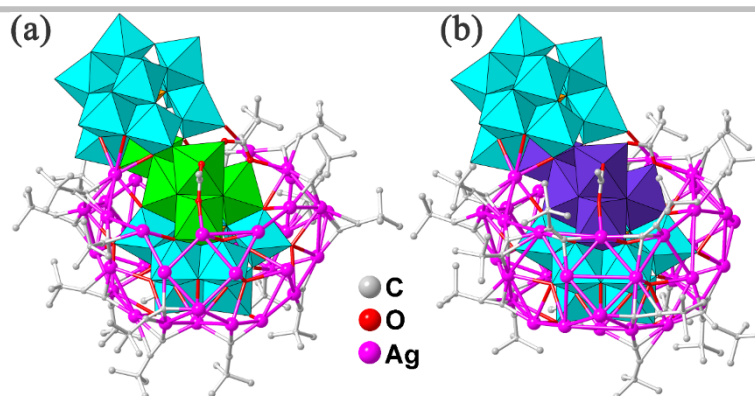


Fig. S5. The structure of Ag<sub>36</sub>-Co (a) and Ag<sub>36</sub>-Ni (b). Polyhedron code: W, cyan; Si, orange; Co, green; Ni, mauve.

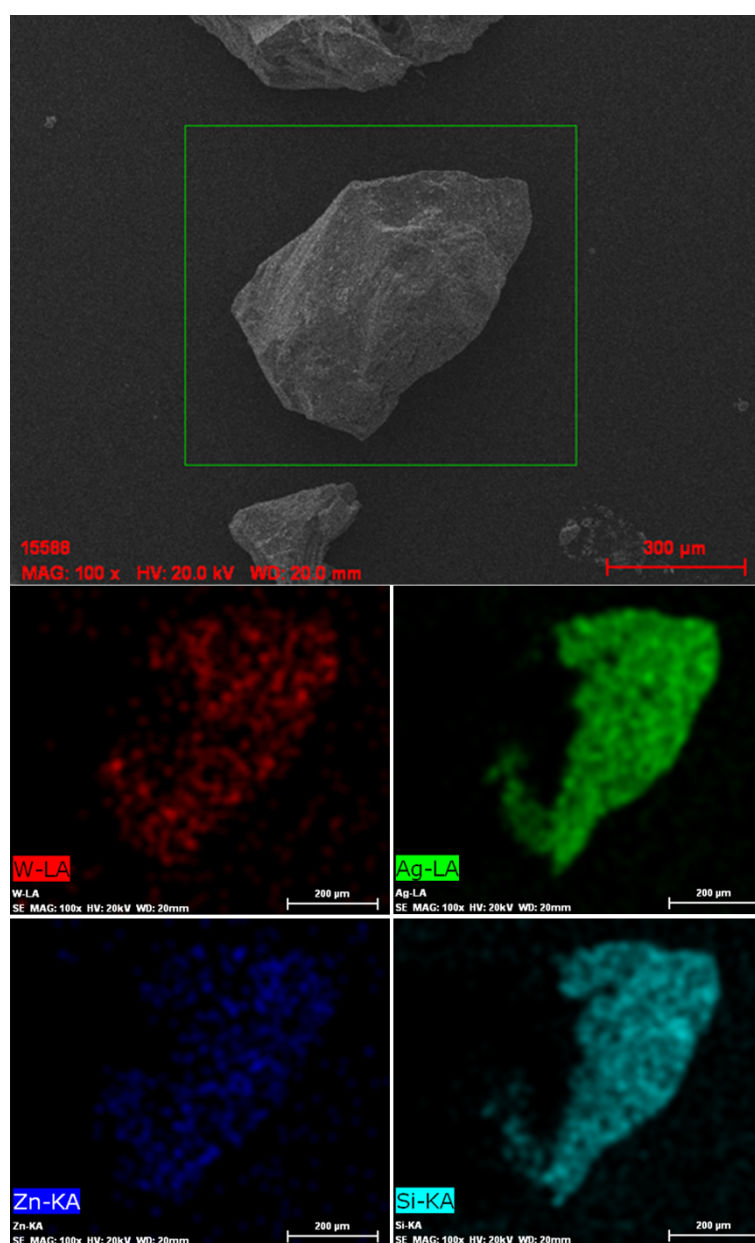
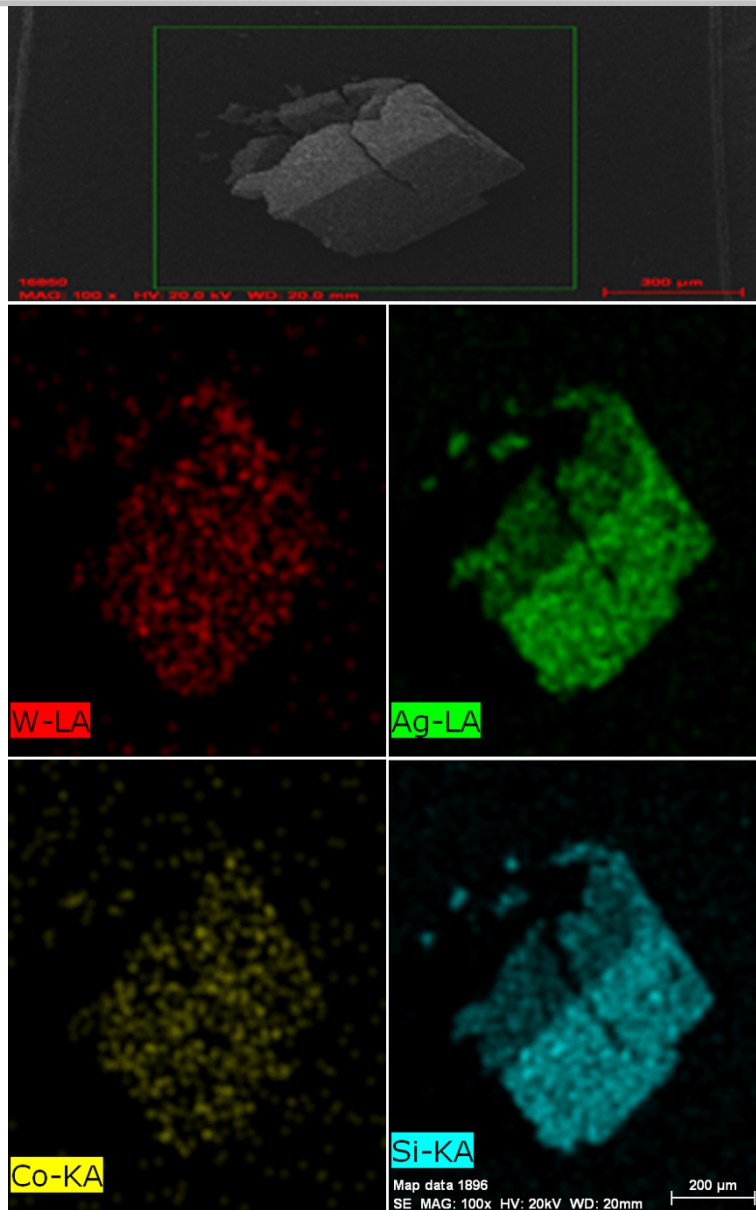
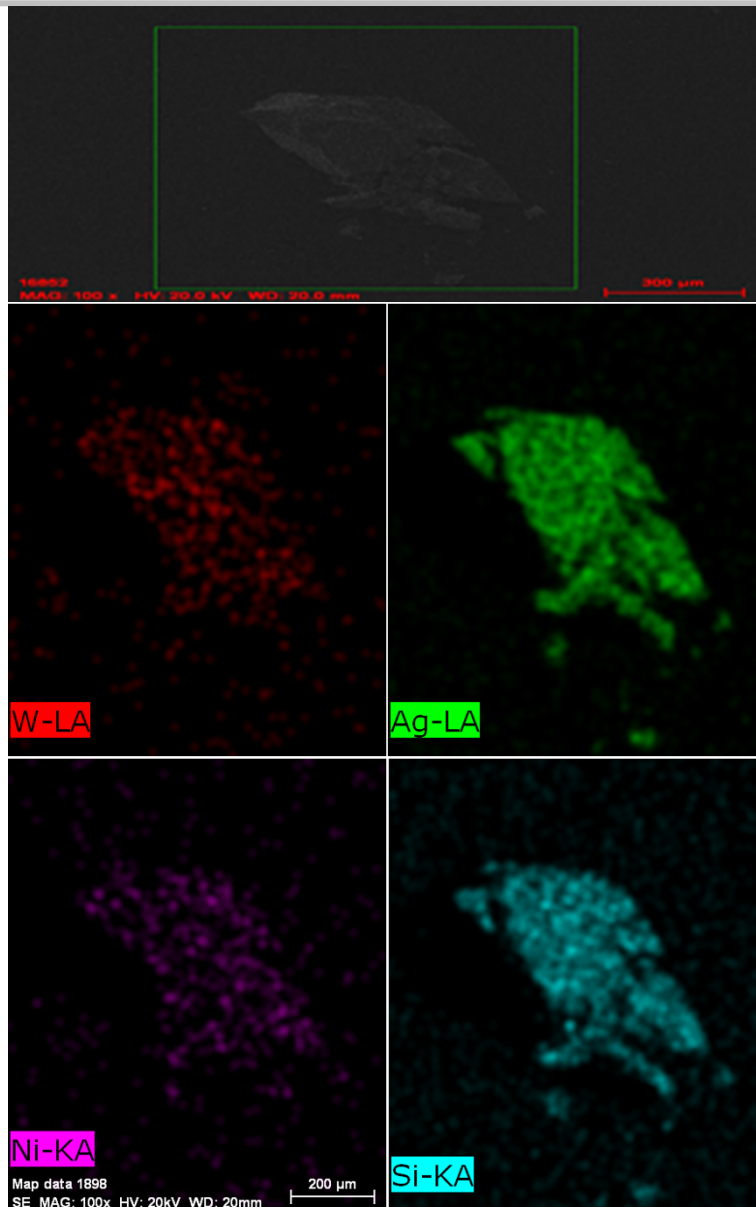


Fig. S6. The element distributions in Ag<sub>38</sub>-Zn based on the EDS elemental mapping.



**Fig. S7.** The element distributions in **Ag<sub>38</sub>-Co** based on the EDS elemental mapping.



**Fig. S8.** The element distributions in **Ag38-Ni** based on the EDS elemental mapping.

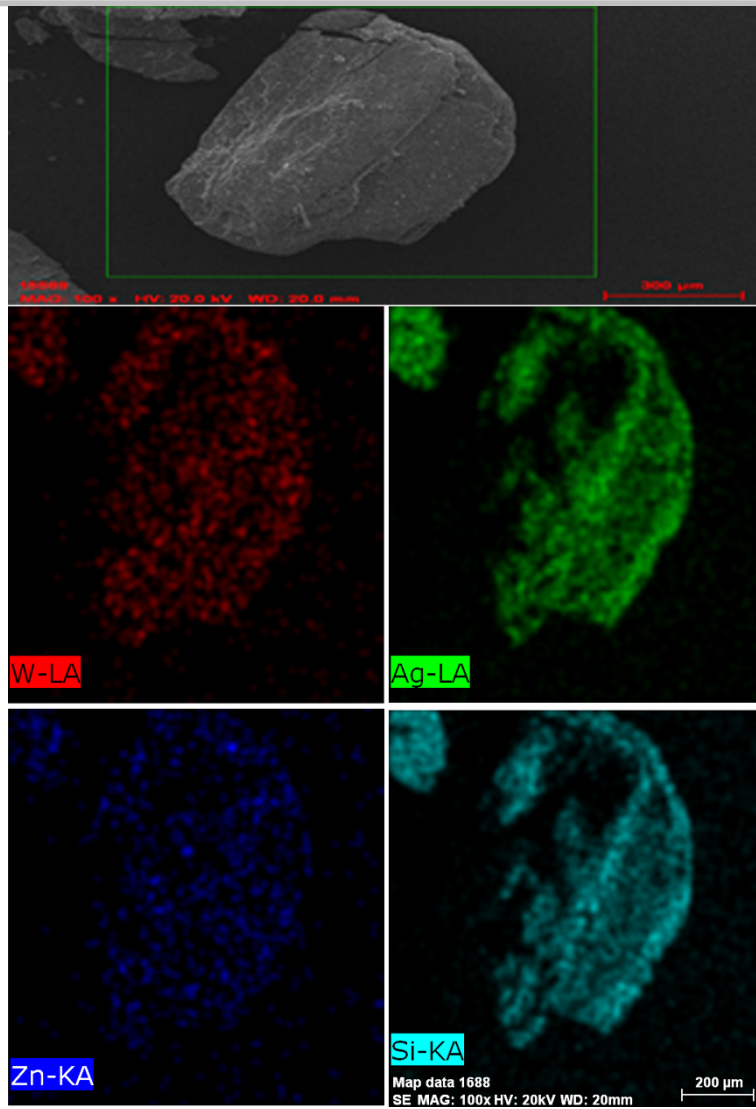
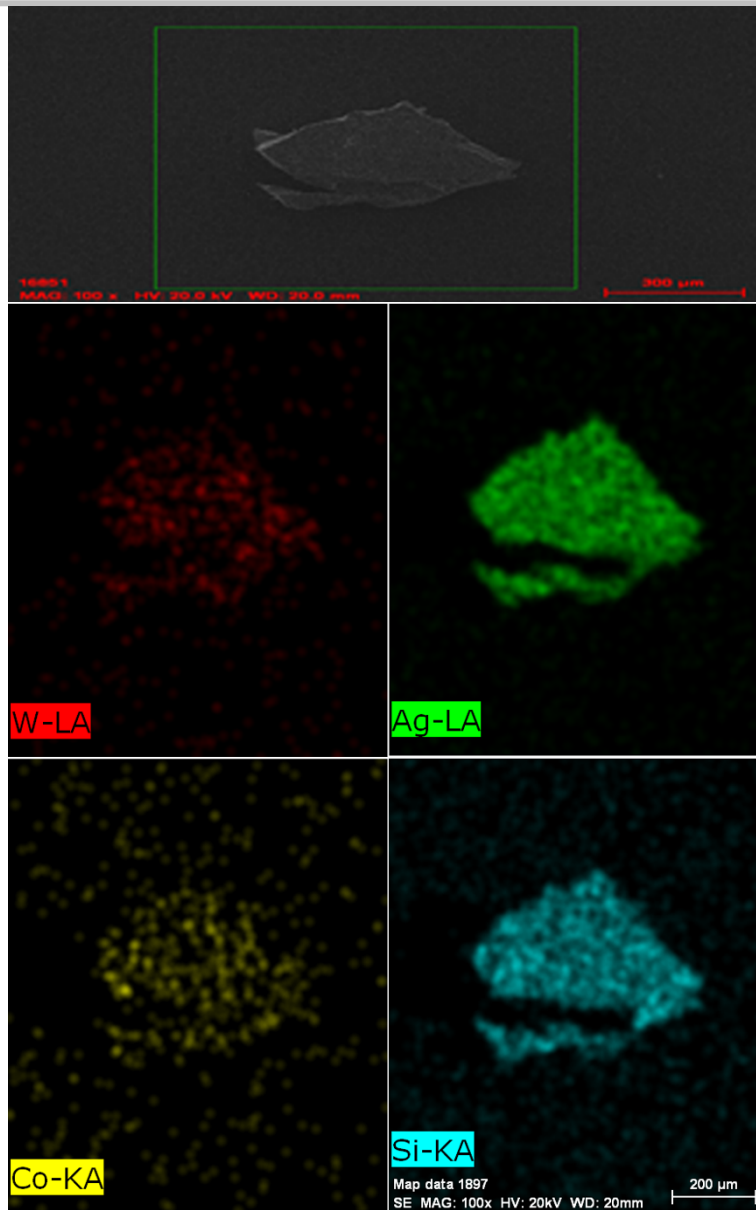


Fig. S9. The element distributions in Ag<sub>37</sub>-Zn based on the EDS elemental mapping.



**Fig. S10.** The element distributions in **Ag<sub>36</sub>-Co** based on the EDS elemental mapping.

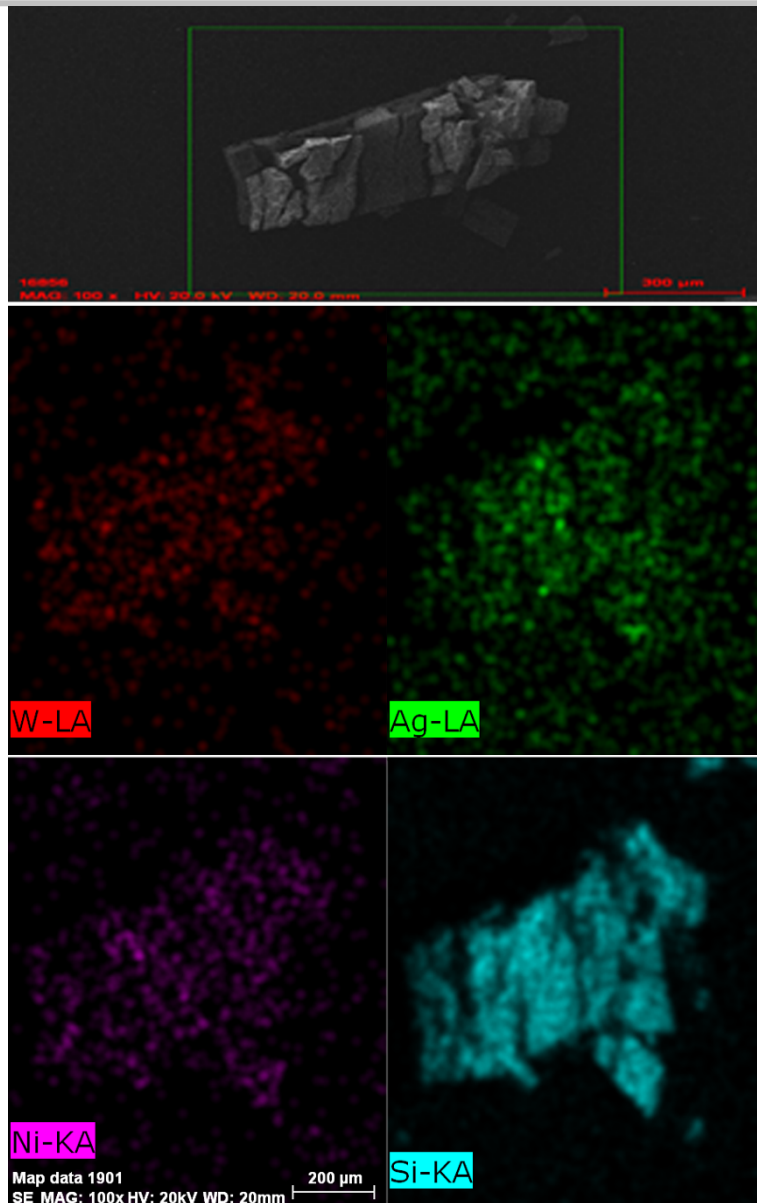
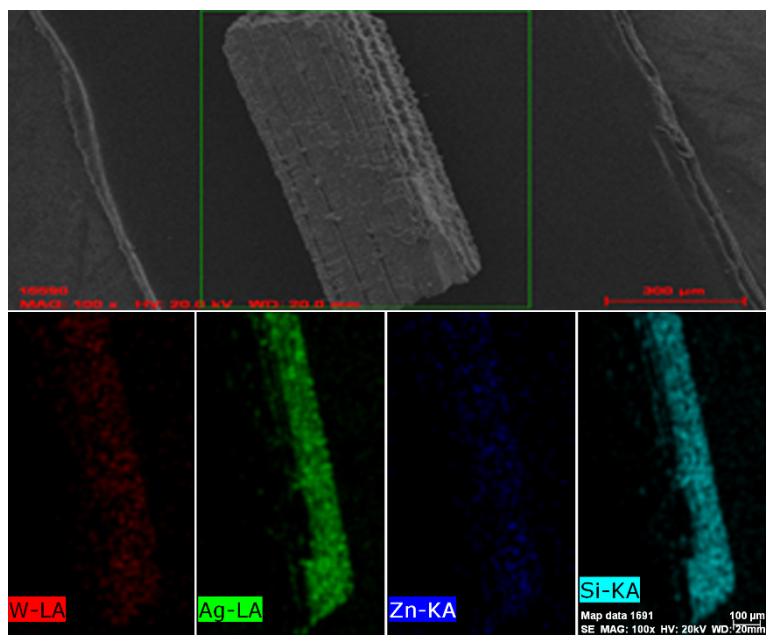
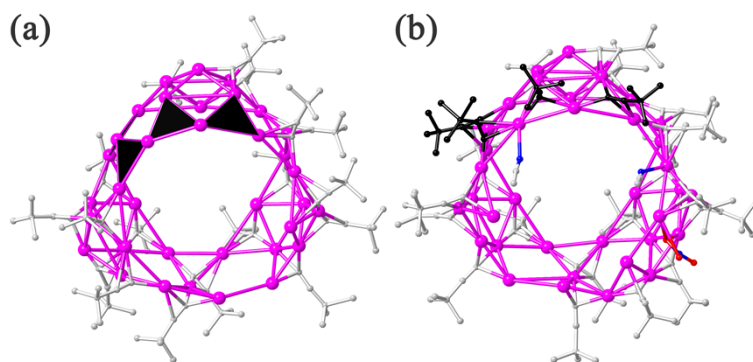


Fig. S11. The element distributions in Ag<sub>36</sub>-Ni based on the EDS elemental mapping.



**Fig. S12.** The element distributions in  $\{\text{Ag37-Zn}\}_\infty$  based on the EDS elemental mapping.



**Fig. S13.** The differences of  ${}^t\text{BuC}\equiv\text{C}$  ligands in  $\text{Ag36-Co}$  (a) and  $\text{Ag37-Zn}$  (b), which are marked in black.

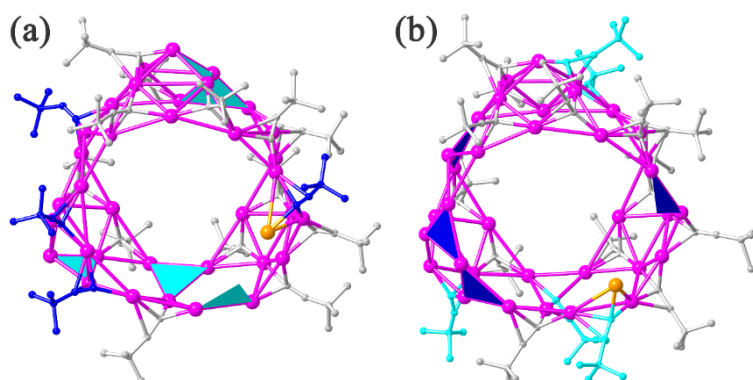


**Fig. S14.** The differences of  ${}^t\text{BuC}\equiv\text{C}$  ligands in  $\text{Ag36-Ni}$  (a) and  $\text{Ag36-Co}$  (b), which are marked in blue and cyan. The difference between the two silver cage is marked in orange.

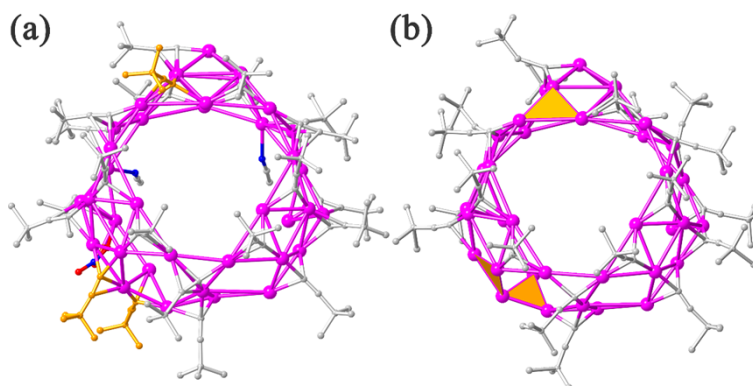


**Fig. S15.** The differences of  ${}^t\text{BuC}\equiv\text{C}$  ligands in  $\text{Ag37-Zn}$  (a) and  $\{\text{Ag37-Zn}\}_\infty$  (b), which are marked in orange.

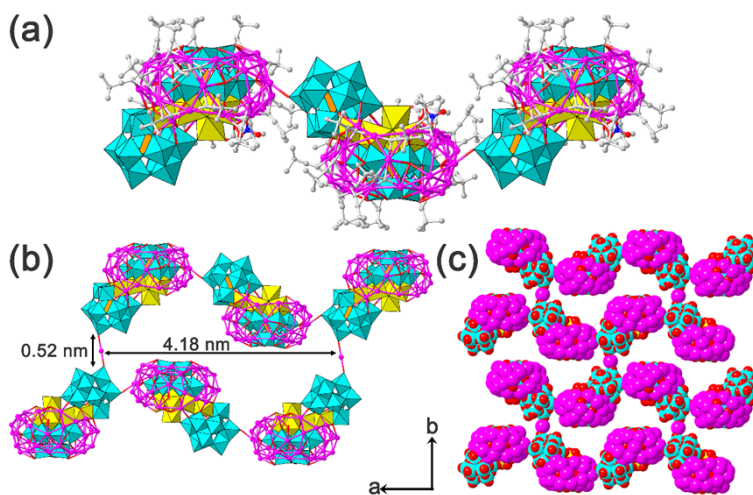


**Fig. S16.** a) The 1D chain in  $\{\text{Ag37-Zn}\}_\infty$ . b) The irregular channel of  $\{\text{Ag37-Zn}\}_\infty$ . c) The 2D layer of  $\{\text{Ag37-Zn}\}_\infty$  under space filling mode. The peripheral ligands were omitted for clarity in b) and c). Polyhedron code: W, cyan; Si, orange; Zn, yellow.

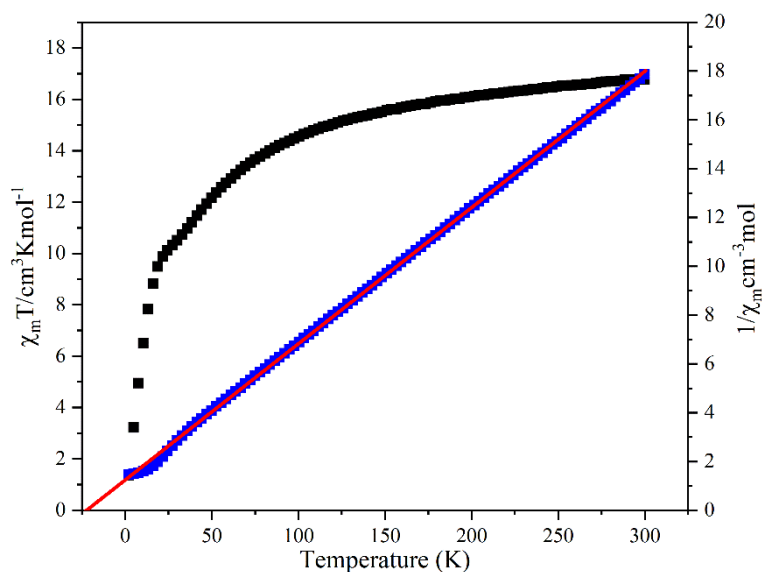


**Fig. S17.** Temperature dependence of  $\chi_m T$  and  $1/\chi_m T$  for  $\text{Ag38-Co}$  in the temperature range of 2-300 K in an applied magnetic field of 1 KOe. The red line represents the least-square fit by using the Curie-Weiss law.

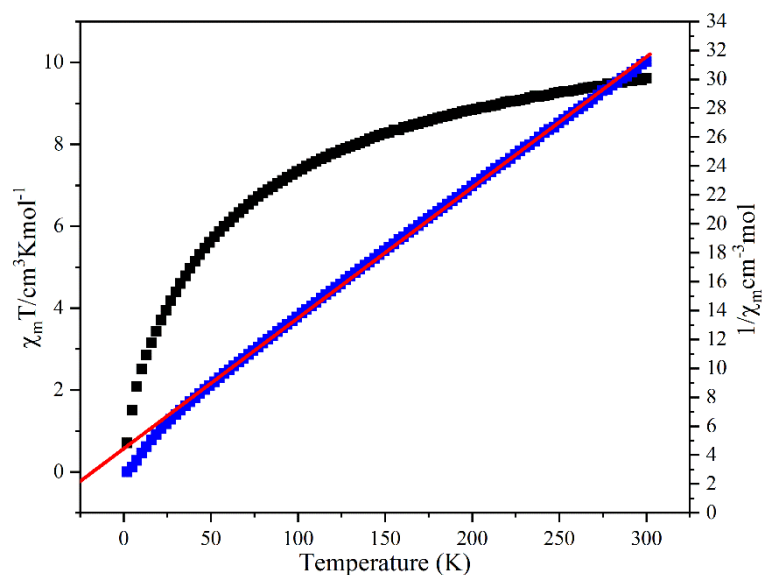


**Fig. S18.** Temperature dependence of  $\chi_m T$  and  $1/\chi_m T$  for  $\text{Ag38-Ni}$  in the temperature range of 2-300 K in an applied magnetic field of 1 KOe. The red line represents the least-square fit by using the Curie-Weiss law.

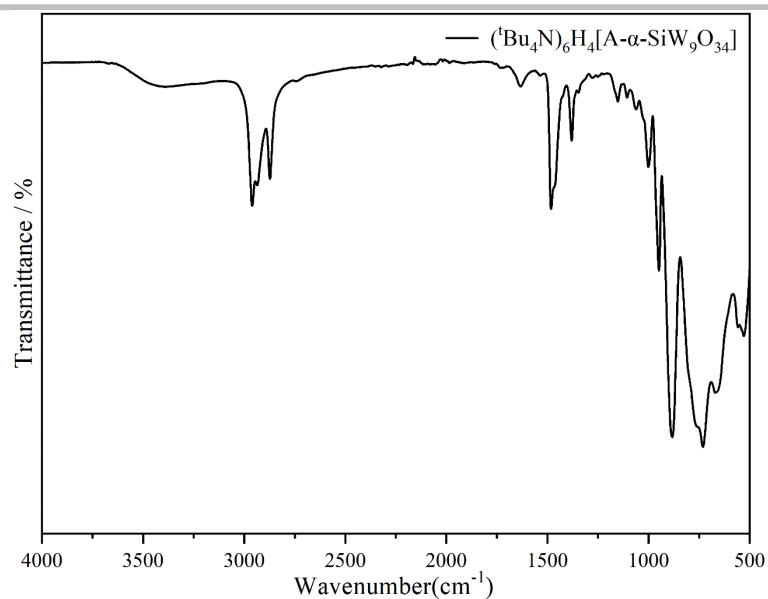


**Fig. S19.** IR spectrum of  $(t\text{Bu}_4\text{N})_6\text{H}_4[\text{SiW}_9\text{O}_{34}]$ .  $\nu_{\text{C-H}}$ :  $\sim 2960 \text{ cm}^{-1}$ ;  $\nu_{\text{C-H(as)}}$ :  $\sim 1482 \text{ cm}^{-1}$ ;  $\nu_{\text{C-H(s)}}$ :  $\sim 1380 \text{ cm}^{-1}$ ;  $\nu_{\text{W-O}}$ :  $\sim 951 \text{ cm}^{-1}$ ,  $\sim 883 \text{ cm}^{-1}$ ,  $\sim 729 \text{ cm}^{-1}$ ,  $\sim 663 \text{ cm}^{-1}$ , and  $\sim 529 \text{ cm}^{-1}$ .

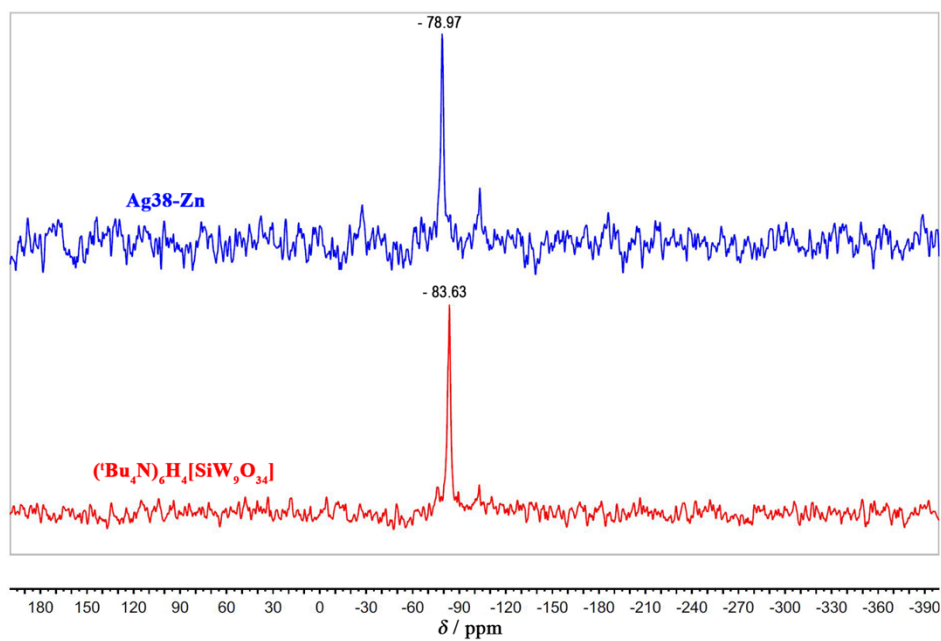


**Fig. S20.** The  $^{29}\text{Si}$  NMR spectra of  $(t\text{Bu}_4\text{N})_6\text{H}_4[\text{SiW}_9\text{O}_{34}]$  and  $\text{Ag}_{38}\text{-Zn}$ .

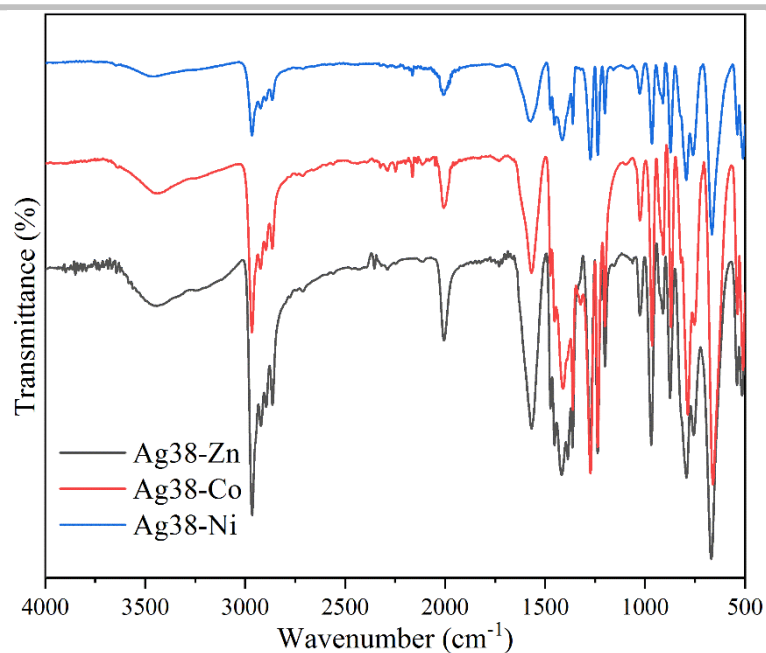


**Fig. S21.** IR spectra of **Ag38-TM**.

The stretching bands of -OH groups are observed at  $\sim 3450\text{ cm}^{-1}$ . The appearance of  $\nu(\text{C-H})$  and  $\nu(\text{C}\equiv\text{C})$  can be confirmed at  $\sim 2966\text{ cm}^{-1}$  and  $2001\text{ cm}^{-1}$ , respectively. The asymmetric vibration bands of C=O groups appear at  $\sim 1624\text{ cm}^{-1}$  and  $1570\text{ cm}^{-1}$ , and the symmetric ones can be found at  $\sim 1469\text{ cm}^{-1}$  and  $1452\text{ cm}^{-1}$ . The vibration bands centered at  $\sim 1380\text{ cm}^{-1}$  and  $840\text{ cm}^{-1}$  are assigned to the resonance bands of nitrates. Moreover, the characteristic vibration bands of W-O groups appear at  $\sim 968\text{ cm}^{-1}$ ,  $869\text{ cm}^{-1}$ ,  $786\text{ cm}^{-1}$ ,  $754\text{ cm}^{-1}$ , and  $659\text{ cm}^{-1}$ .<sup>[6-8]</sup>

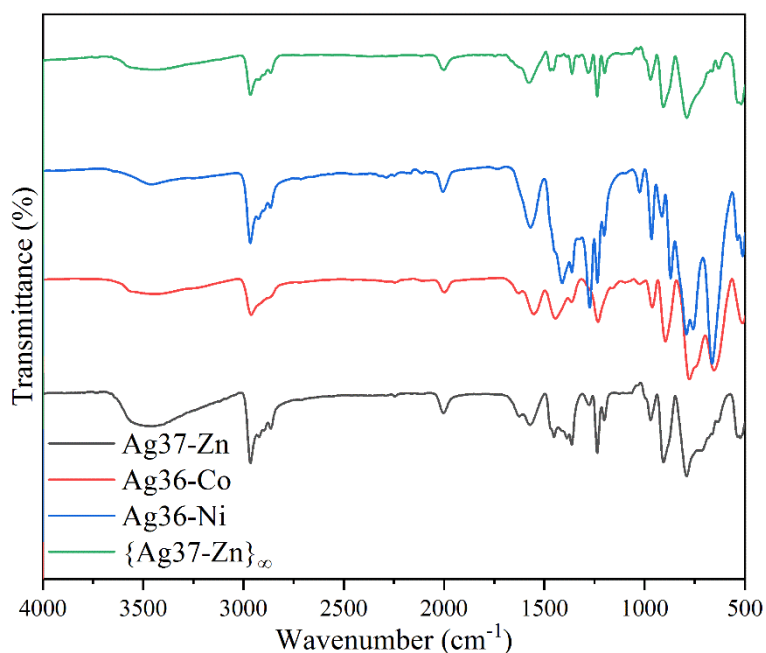


**Fig. S22.** IR spectra of **Ag37-Zn**, **Ag36-TM**, and **{Ag37-Zn}∞**.

The stretching bands of -OH groups are observed at  $\sim 3500\text{ cm}^{-1}$ . The appearance of  $\nu(\text{C-H})$  and  $\nu(\text{C}\equiv\text{C})$  can be confirmed at  $\sim 2965\text{ cm}^{-1}$  and  $2003\text{ cm}^{-1}$ , respectively. The asymmetric vibration bands of C=O groups appear at  $\sim 1627\text{ cm}^{-1}$  and  $1569\text{ cm}^{-1}$ , and the symmetric ones can be found at  $\sim 1473\text{ cm}^{-1}$  and  $1452\text{ cm}^{-1}$ . The vibration bands centered at  $1388\text{ cm}^{-1}$  is assigned to the resonance bands of nitrates (only appears in **Ag37-Zn** and **{Ag37-Zn}∞**). Moreover, the characteristic vibration bands of W-O groups appear at  $971\text{ cm}^{-1}$ ,  $900\text{ cm}^{-1}$ ,  $790\text{ cm}^{-1}$ ,  $786\text{ cm}^{-1}$ , and  $661\text{ cm}^{-1}$ .<sup>[6-8]</sup>

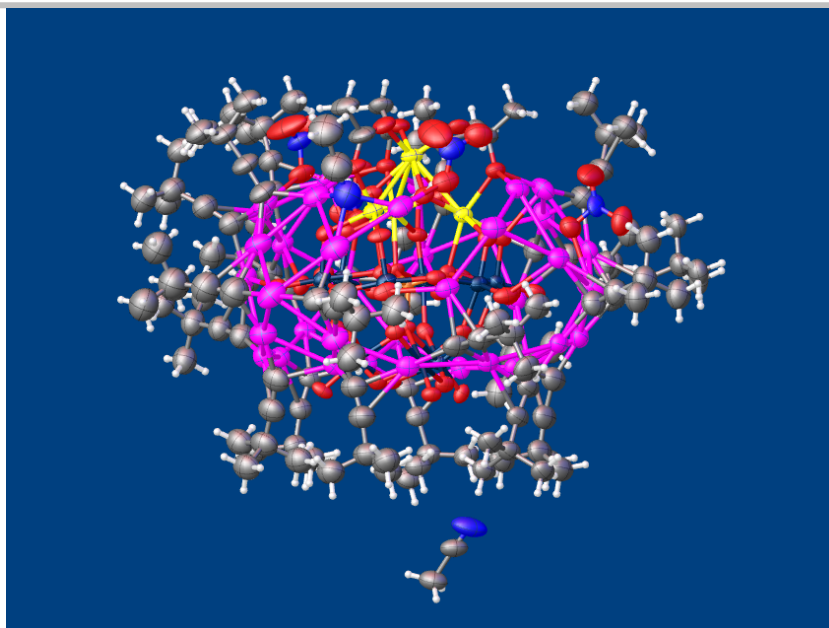


**Fig. S23.** The ellipsoid mode of **Ag38-Zn**.

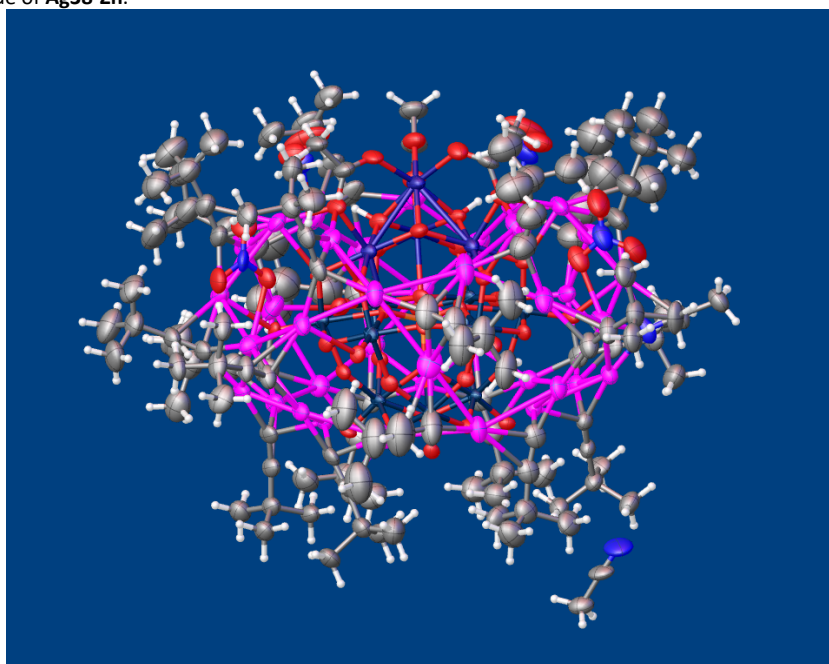


**Fig. S24.** The ellipsoid mode of **Ag38-Co**.

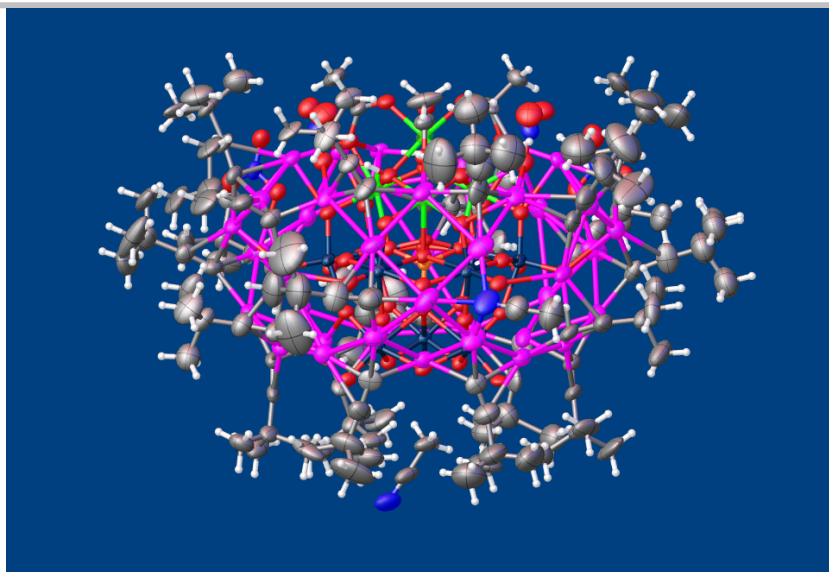


Fig. S25. The ellipsolid mode of Ag<sub>38</sub>-Ni.

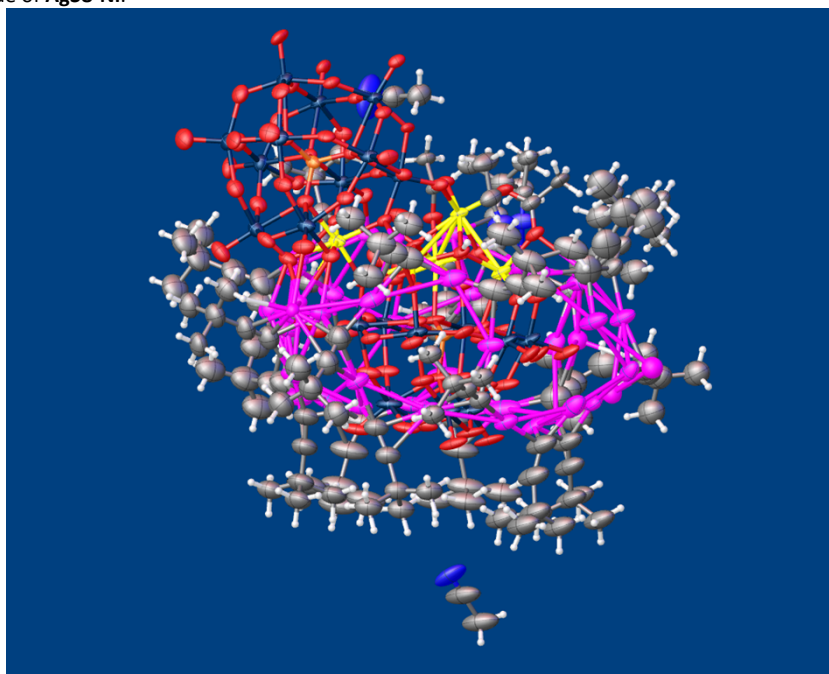
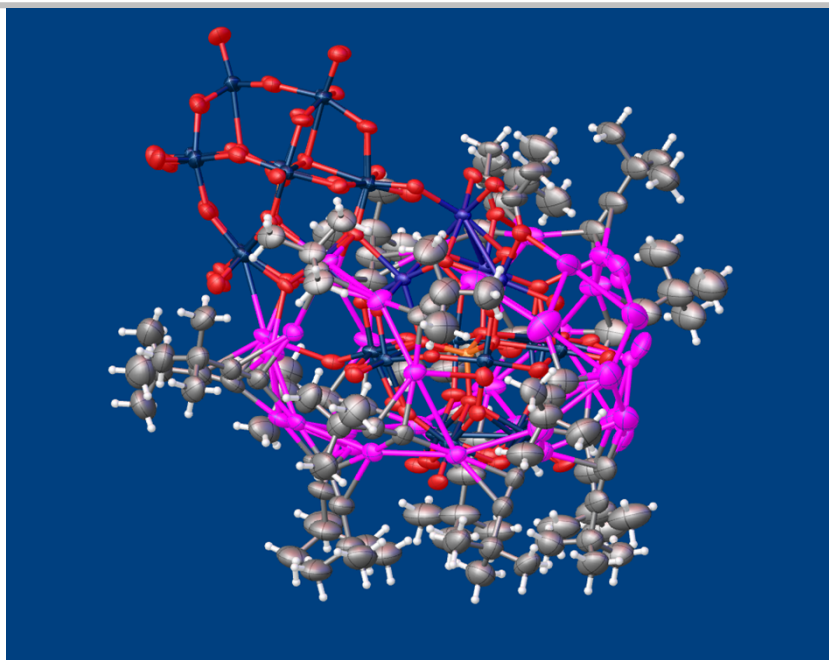
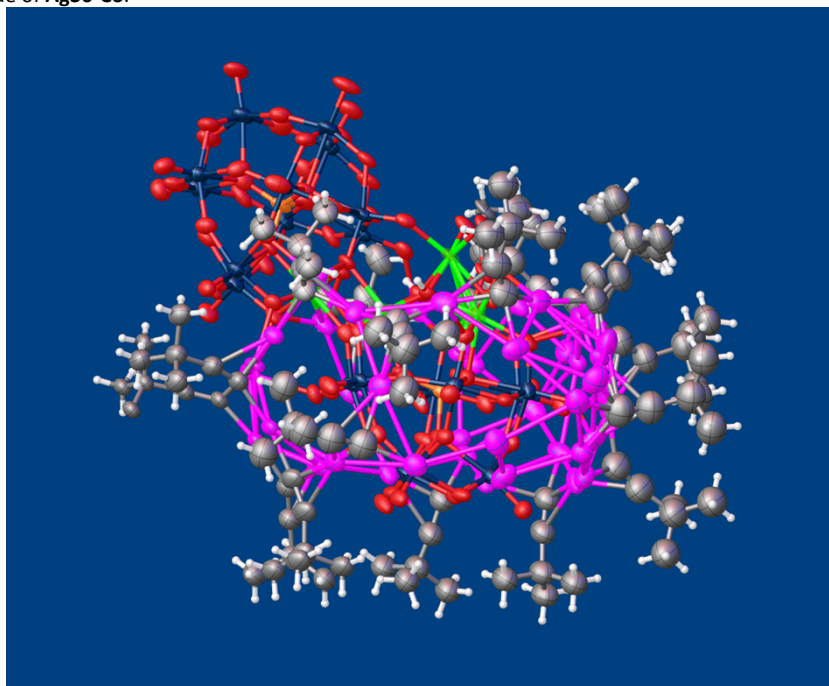


Fig. S26. The ellipsolid mode of Ag<sub>37</sub>-Zn.



**Fig. S27.** The ellipsoid mode of **Ag36-Co**.



**Fig. S28.** The ellipsoid mode of **Ag36-Ni**.

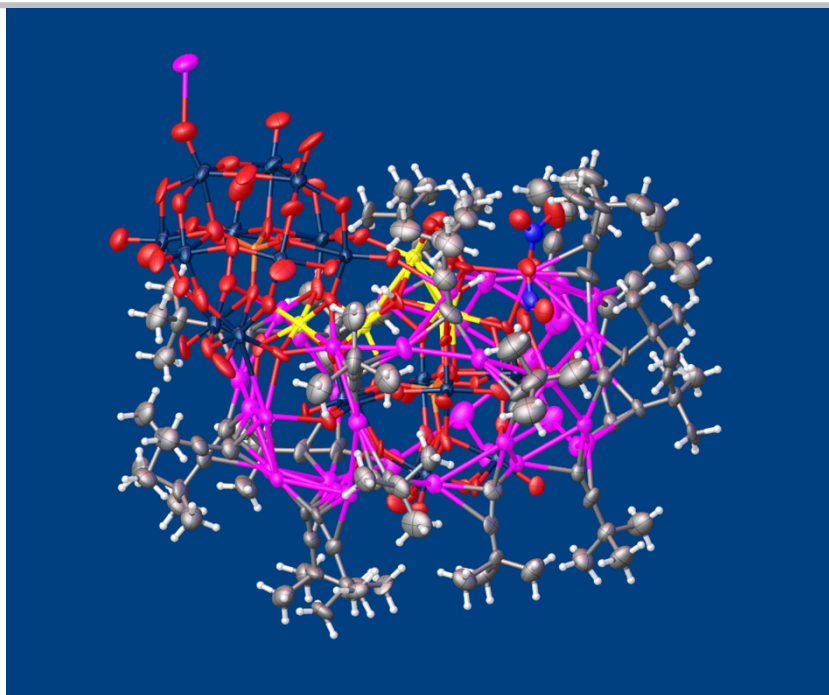


Fig. S29. The ellipsoid mode of  $\{\text{Ag}_{37}\text{-Zn}\}_{\infty}$ .

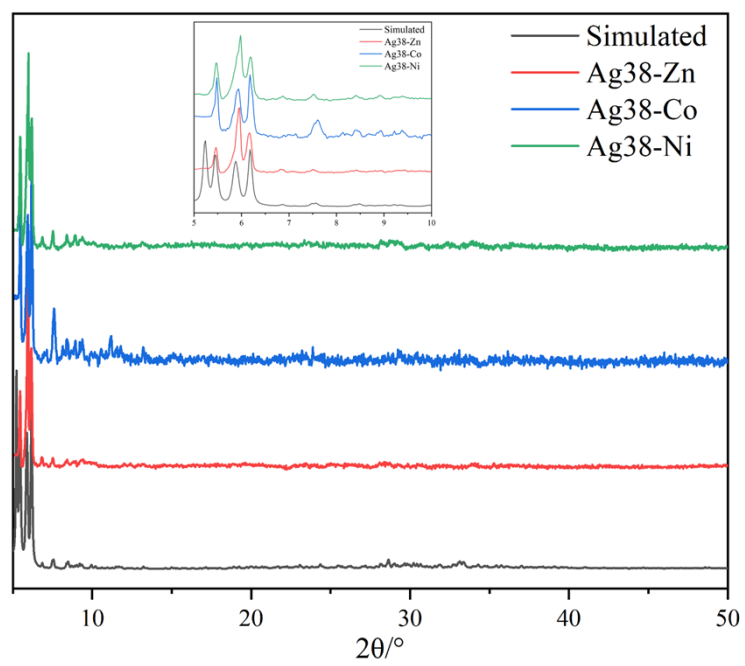
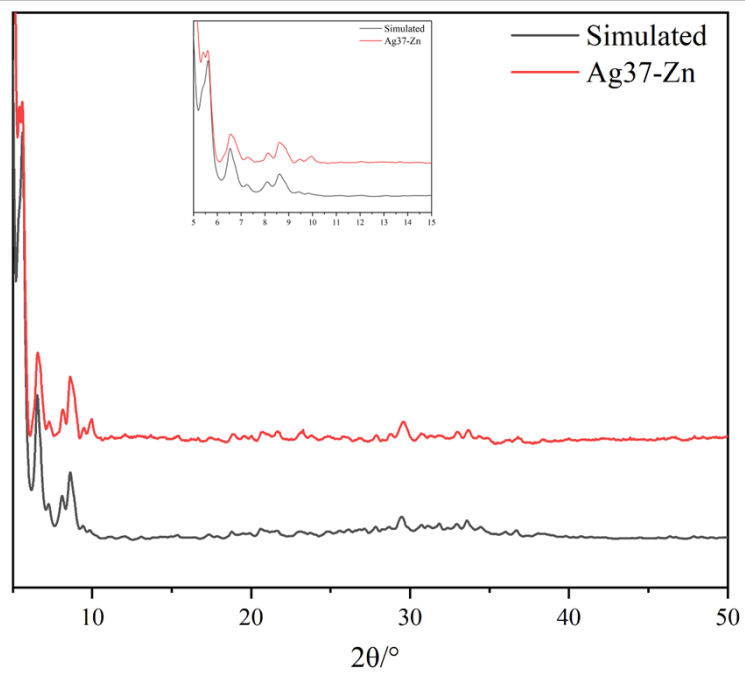
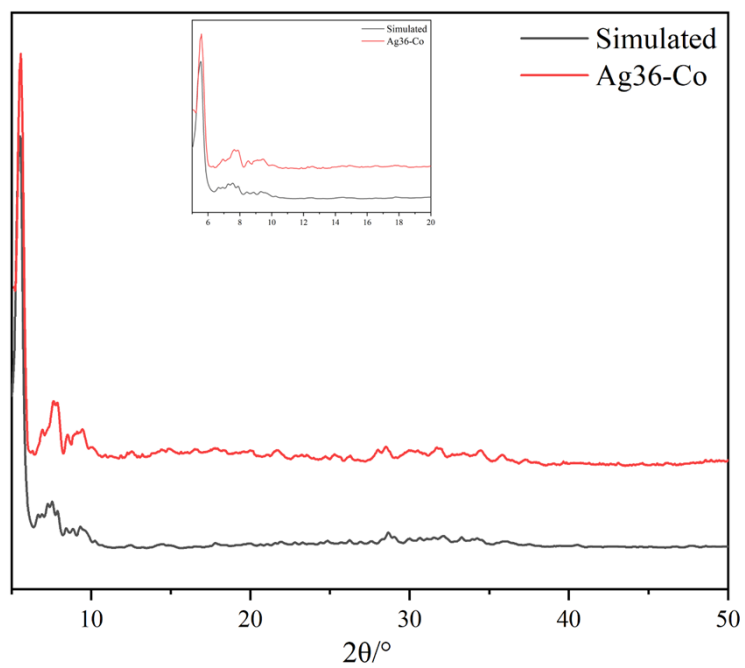


Fig. S30. Simulated and experimental PXRD patterns of  $\text{Ag}_{38}\text{-TM}$ .



**Fig. S31.** Simulated and experimental PXRD patterns of **Ag<sub>37</sub>-Zn**.



**Fig. S32.** Simulated and experimental PXRD patterns of **Ag<sub>36</sub>-Co**.

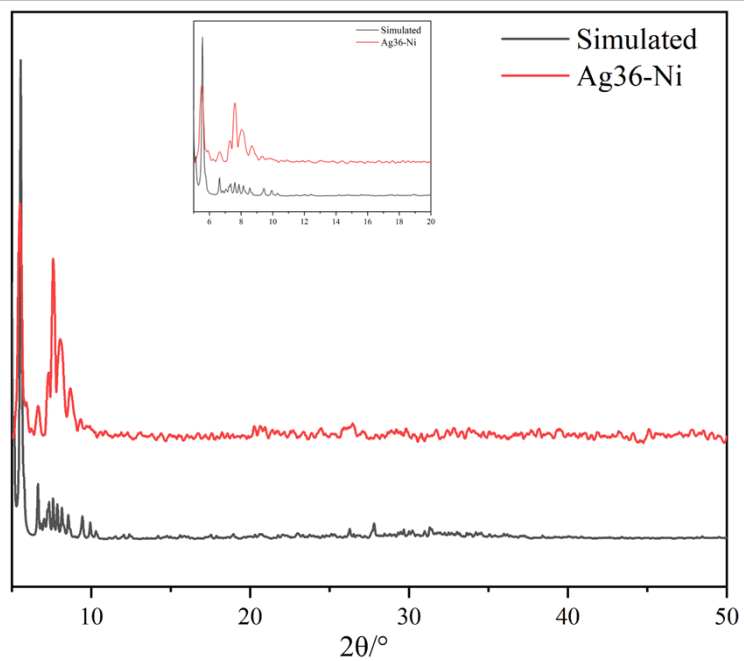


Fig. S33. Simulated and experimental PXRD patterns of **Ag<sub>36</sub>-Ni**.

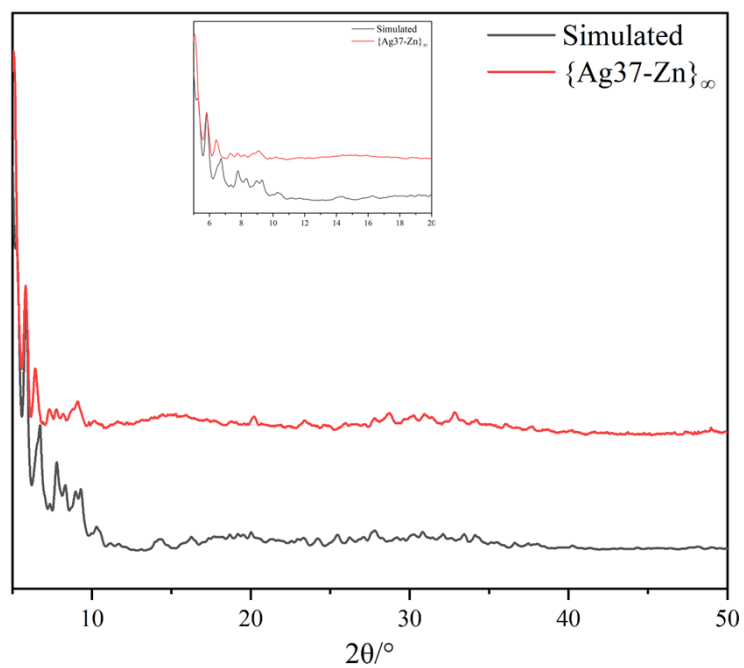
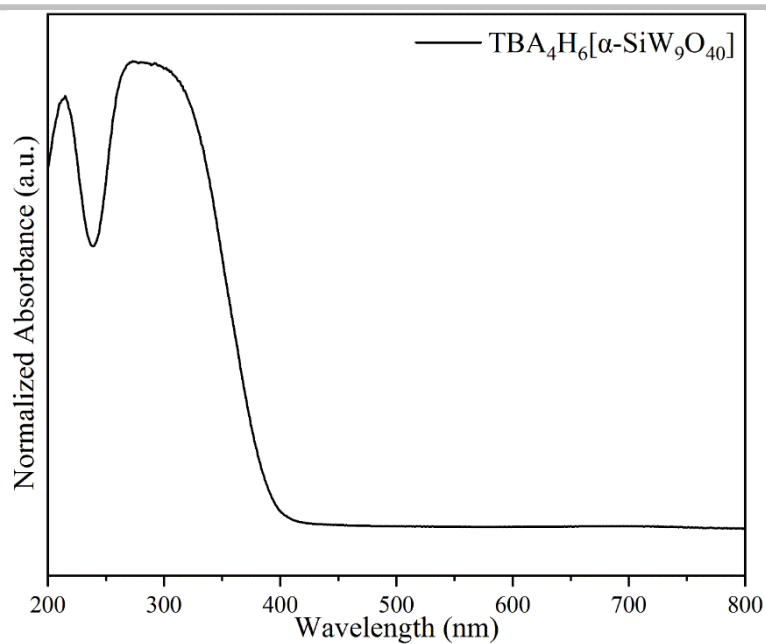
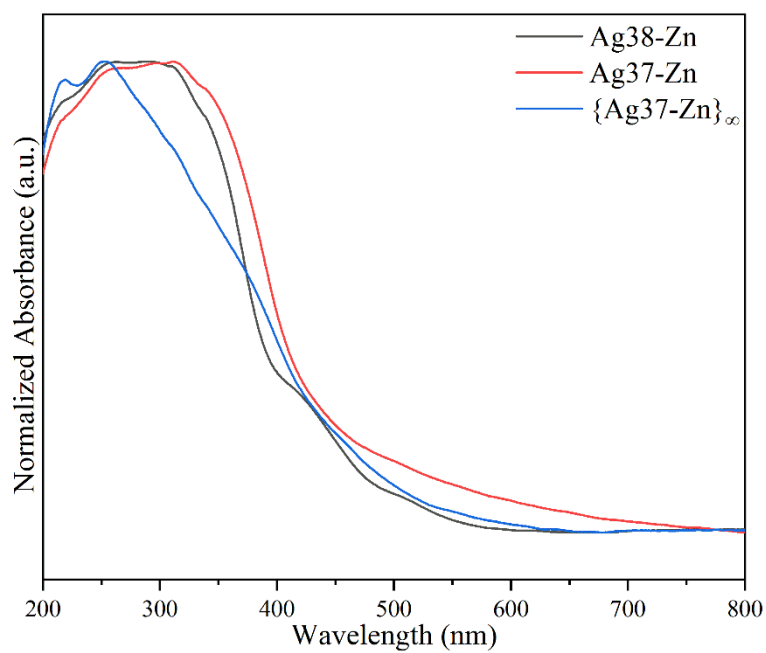


Fig. S34. Simulated and experimental PXRD patterns of **{Ag<sub>37</sub>-Zn}<sub>∞</sub>**.



**Fig. S35.** UV-vis absorption spectra of the  $(\text{tBu}_4\text{N})_6\text{H}_4[\text{SiW}_9\text{O}_{34}]$  precursor. The absorption bands centered at 230 and 300 nm are originated from the  $p\pi(\text{O}) \rightarrow d\pi^*(\text{W})$  transition.<sup>[9]</sup>



**Fig. S36.** UV-vis absorption spectra of  $\text{Ag38-Zn}$ ,  $\text{Ag37-Zn}$ , and  $\{\text{Ag37-Zn}\}_\infty$ . The absorption bands centered at  $\sim 300$  nm are originated from the  $p\pi(\text{O}) \rightarrow d\pi^*(\text{W})$  transition in the POM template.<sup>[9]</sup>

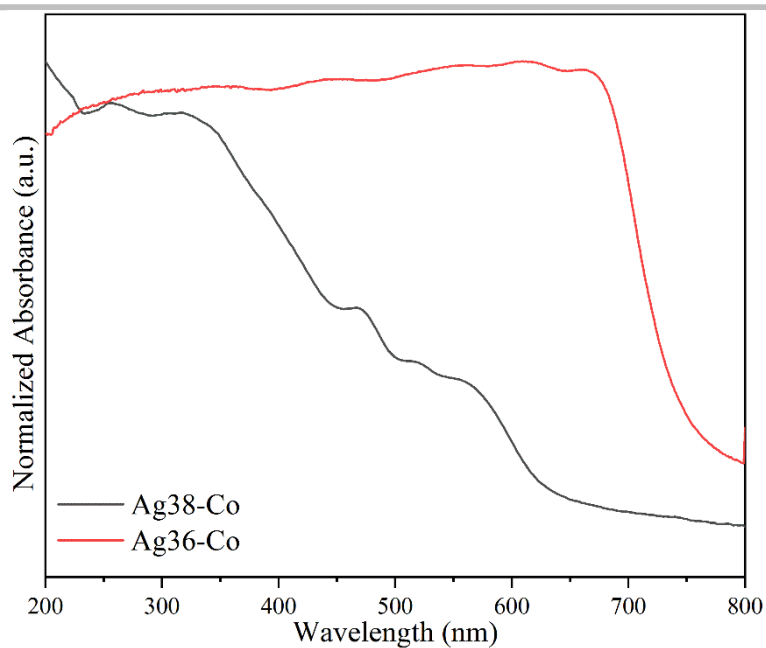


**Fig. S37.** UV-vis absorption spectra of **Ag38-Co** and **Ag36-Co**. The absorption of **Ag36-Co** centered at 310 nm is originated from the  $\rho\pi(O) \rightarrow d\pi^*(W)$  transition in the POM template, and the shoulder band centered at 550 nm can be attributed to the  $d \rightarrow d$  transition from the  $Co^{2+}$  ions. The broad absorption band of **Ag36-Co** can be assigned to the cooperation of the  $\rho\pi(O) \rightarrow d\pi^*(W)$  transition in the POM template and the  $d \rightarrow d$  transition from the  $Co^{2+}$  ions.<sup>[10]</sup>

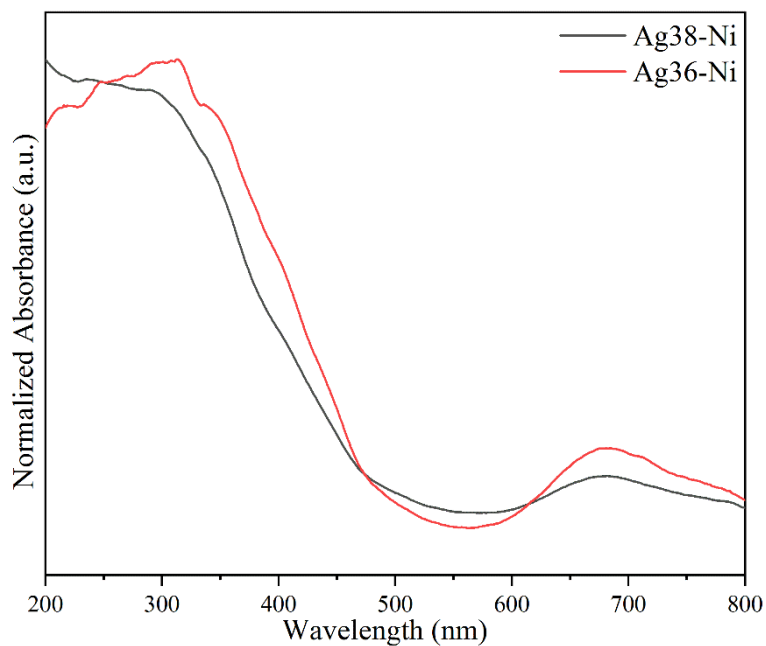


**Fig. S38.** UV-vis absorption spectra of **Ag38-Ni** and **Ag36-Ni**.

Both of the absorption bands centered at  $\sim 310$  nm and  $\sim 670$  nm can be assigned to the cooperation of the  $\rho\pi(O) \rightarrow d\pi^*(W)$  transition in the POM template and the  $d \rightarrow d$  transition from the  $Ni^{2+}$  ions, respectively.<sup>[10]</sup>

### 3. Tables

Table S1 The bond valence of the incorporated transition metal ions in the POM templates

Compound	Transition metal ions	Valence
Ag38-Zn	Zn1	2.104
	Zn2	2.149
	Zn3	2.098
	Zn4	2.166
Ag38-Co	Co1	2.055
	Co2	1.932
	Co3	2.142
	Co4	2.011
Ag38-Ni	Ni1	2.003
	Ni2	2.033
	Ni3	2.053
	Ni4	1.955
Ag37-Zn	Zn1	2.077
	Zn2	2.180
	Zn3	2.055
	Zn4	2.034
	Zn5	2.076
{Ag37-Zn} <sub>∞</sub>	Zn1	1.978
	Zn2	1.928
	Zn3	2.026
	Zn4	2.200
	Zn5	2.179
Ag36-Co	Co1	2.034
	Co2	1.958
	Co3	2.081
	Co4	2.127
	Co5	2.094
Ag36-Ni	Ni1	1.780
	Ni2	1.956
	Ni3	1.963
	Ni4	1.781
	Ni5	1.905

---

## 4. References

- [1] Z.-G. Jiang, K. Shi, Y.-M. Lin, Q.-M. Wang, *Chem. Commun.* 2014, **50**, 2353-2355.
- [2] A. P. Ginsberg, *Inorganic Syntheses, Vol. 27*, Wiley-VCH, Weinheim, 1990.
- [3] T. Minato, K. Suzuki, K. Kamata, and N. Mizuno, *Chem. Eur. J.* 2014, **20**, 5946–5952.
- [4] Z.-R. Yuan, Z. Wang, B.-L. Han, C.-K. Zhang, S.-S. Zhang, Z.-Y. Zhu, J.-H. Yu, T.-D. Li, Y.-Z. Li, C.-H. Tung and D. Sun, *Angew. Chem. Int. Ed.*, 2022, **61**, e202211628.
- [5] Z. Wang, Y.-J. Zhu, Y.-Z. Li, G.-L. Zhuang, K.-P. Song, Z.-Y. Gao, J.-M. Dou, M. Kurmoo, C.-H. Tung and D. Sun, *Nat. Comm.* 2022, **13**, 1802.
- [6] F. Gruber and M. Jansen, *Angew. Chem. Int. Ed.*, 2010, **49**, 4924-4926.
- [7] K.-G. Liu, X.-Y. Liu, Z.-J. Guan, K. Shi, Y.-M. Lin and Q.-M. Wang, *Chem. Commun.*, 2016, **52**, 3801-3804.
- [8] L. Lisnard, P. Mialane, A. Dolbecq, J. Marrot, J. M. Clemente-Juan, E. Coronado, B. Keita, P. de Oliveira, L. Nadjo and F. Sécheresse, *Chem. Eur. J.*, 2007, **13**, 3525-3536.
- [9] S.-S. Zhang, J.-Y. Chen, K. Li, J.-D. Yuan, H.-F. Su, Z. Wang, M. Kurmoo, Y.-Z. Li, Z.-Y. Gao, C.-H. Tung, D. Sun, L. Zheng, *Chem. Mater.* 2021, **33**, 9708-9714.
- [10] V. W.-W. Yam, V. K.-M. Au, S. Y.-L. Leung, *Chem. Rev.* 2015, **115**, 7589-7728.